Received: 12 October 2024 | Revised: 12 February 2025 | Accepted: 28 February 2025

DOI: 10.1002/alz.70122

Alzheimer's & Dementia®
THE JOURNAL OF THE ALZHEIMER'S ASSOCIATION

RESEARCH ARTICLE

Cerebral proteome adaptations to amyloid angiopathy are prevented by carbonic anhydrase inhibitors

Jasper Carlsen[1] | **Silvia Fossati**[2] | **Leif Østergaard**[3] | **Eugenio Gutiérrez-Jiménez**[3] | **Johan Palmfeldt**[1]

[1]Research Unit for Molecular Medicine (MMF), Department of Clinical Medicine, Aarhus University, Aarhus N, Denmark

[2]Alzheimer's Center at Temple (ACT) and Department of Neural Sciences, Temple University, Philadelphia, Pennsylvania, USA

[3]Center of Functionally Integrative Neuroscience (CFIN), Department of Clinical Medicine, Aarhus University, Aarhus N, Denmark

Correspondence
Johan Palmfeldt, Research Unit for Molecular Medicine (MMF), Department of Clinical Medicine, Aarhus University, Olof Palmes Alle 49, DK-8200, Aarhus N, Denmark.
Email: johan.palmfeldt@clin.au.dk

Eugenio Jiménez-Gutiérrez, Center of Functionally Integrative Neuroscience (CFIN), Department of Clinical Medicine, Aarhus University, Palle Juul-Jensens Boulevard 99, DK-8200 Aarhus N, Denmark.
Email: EUGENIO@CFIN.AU.DK

Funding information
Alzheimer's Association, Grant/Award Number: AARF-18-564411; VELUX Foundation, Grant/Award Number: 0026167; Lundbeck Foundation, Grant/Award Number: R310-2018-3455

Abstract

BACKGROUND: Cerebral amyloid angiopathy (CAA) is a hallmark of Alzheimer's disease (AD), linked to adverse effects of emerging AD treatments. We explored the molecular effects of CAA in mouse brain and evaluated how these could be prevented by two repurposed United States Food and Drug Administration (FDA) approved treatments.

METHODS: Brain proteomics was performed on the Tg-SwDI genetic mouse model carrying disease causing mutations and developing AD characteristic cognitive deficits and severe CAA. Cortical and hippocampal tissues from presymptomatic male and female mice were studied.

RESULTS: We identify a core of dysregulated proteins across studies, including established markers of AD as well as proteins indicative of astrogliosis and negative regulators of synaptic stability and function. Two FDA approved, repurposed carbonic anhydrase inhibitors (CAIs), acetazolamide and methazolamide, were effective in preventing these molecular adaptations.

DISCUSSION: The two drugs broadly prevent proteome adaptations to the detrimental genotype and retain glutamatergic synapse proteins significantly closer to wild-type levels.

KEYWORDS
Alzheimer's disease, Arp2/3, biomarker, cerebral amyloid angiopathy, complement, cortex, Ephexin-1, glutamatergic synapse, hippocampus, neurodegenerative disease, proteome, Tg-SwDI mouse model

Highlights

- The brain proteome changes of mice with CAA are mapped.
- Cortical and hippocampal tissues from presymptomatic male and female mice are studied.

Eugenio Gutiérrez-Jiménez and Johan Palmfeldt both authors contributed equally to the manuscript.

- Markers of AD, astrogliosis, and synaptic stability are dysregulated.
- Two CAI are effective in preventing these protein changes.

1 | BACKGROUND

The prevalence of dementia is increasing rapidly and Alzheimer's disease (AD) is a significant part of this problem constituting 60-80% of dementia cases.[1,2] AD is characterized clinically by progressive cognitive decline and memory loss and molecularly by the deposition of amyloid β peptide (Aβ) and of hyperphosphorylated tau protein.[3]

Aβ peptides aggregate in senile plaques and around cerebral vessels[4,5] The deposition of Aβ in vessel walls – cerebral amyloid angiopathy (CAA) – has become a greater matter of interest, as it has become clear that dementia and cardiovascular disease are closely linked, and that CAA may bridge this connection.[6,7] CAA and AD can occur independently of each other, but 50% of AD patients have moderate-to-severe CAA compared to 6% of the cognitively normal elderly population,[8] and 90% of AD patients display CAA upon autopsy.[9] CAA destabilizes the blood brain barrier and the vessel malleability and integrity, which additionally impedes perivascular clearance of soluble waste, including Aβ, resulting in a self-perpetuating aggravation of the Aβ pathology[10,11] The pathological changes from CAA correlate with reduced cognitive function,[12] and CAA and classic parenchymal AD pathology have been reported in concert to produce supra-additive rate of cognitive decline.[13]

The Tg-SwDI mouse model was established by Davis et al. to explore CAA as an aspect of AD pathology.[14] Tg-SwDI mice expresses human transgenic mutant APP with two strongly vasculotropic mutations: The Dutch (APP E693Q) and the Iowa (APP D694N) mutations, as well as the Swedish familial AD mutation (APP K670N/M671L).[14] The model develops limited and diffuse parenchymal Aβ deposition, and severe CAA with characteristic accumulation of Aβ peptide around cerebral vessels, together with local inflammation, decreased microvessel density and cognitive impairment similar to AD.[15] Recent reports in this model find only mild cognitive impairment before 12 months,[16,17] and in line with this, we recently found Tg-SwDIs mice ability in completing the Barnes maze task reduced at 15 months[18] but not at 9 months.[19] While specific aspects of molecular pathology in this model are well described, the model has only been subject to proteome and transcriptome analyses of the cerebral vasculature.[20,21] The lack of further omics analyses, not least of the changes in the underlying brain parenchyma, presents a significant information gap considering the model's widespread application for testing novel treatment strategies.[18,22–31]

Recently two immunotherapies have been approved as AD treatments by the FDA but their use is challenging due to their tendency to produce adverse events of abnormal fluid accumulation, microhemorrhages, and edema in the brain, referred to as amyloid-related imaging abnormalities (ARIA).[32] ARIA is related to CAA pathology[33–35]; thus, research into drugs able to modify CAA is highly warranted, as such drugs might both modify cognitive decline directly and reduce complications from immunotherapy.

Carbonic anhydrase inhibitors (CAIs) are FDA approved drugs, for diagnoses such as epilepsy, glaucoma, and mountain sickness.[36] Particularly acetazolamide (AZT) and methazolamide (MTZ) are attractive candidates to modulate vascular pathology in AD. AZT has been shown to improve hemodynamics in the inherited blood vessel disease CADASIL[37]. Furthermore, Both ATZ and MTZ prevent amyloid-induced vascular and neural damage in vitro, through prevention of mitochondrial dysfunction in multiple brain cell types, including cerebral microvascular endothelial cells, brain vascular smooth muscle cells, glial cells, and neuronal cells.[38–41] Furthermore, a recent in vivo study showed that CAI prevent vascular damage and cognitive impairment in 15 month old Tg-SwDI mice.[18] Finally, the pharmacokinetics and safety profiles of ATZ and MTZ indicate that they are suitable for long-term administration and capable of crossing the blood-brain barrier.[42]

In the present study, we validate and extend on the findings of Canepa et al.[18] First, we study the cortical and hippocampal proteome of the Tg-SwDI model and describe in depth the molecular changes and how molecular drivers of astroglial activation and synaptic dysfunction are profoundly dysregulated early in disease progression. Second, we show that preventive treatment with CAIs relieves the proteome-wide adaptations with preventive effects on the synaptic and astroglial pathology.

2 | METHODS

2.1 | Animal models

The study employed homozygous mice from the Tg-SwDI line (C57BL/6-Tg(Thy1-APPSwDutIowa)BWevn/Mmjax). Breeders were acquired from the Mutant Mouse Resource and Research Center (MMRRC Stock No: 34843-JAX). The control group was wild-type (WT) C57Bl/6J mice also acquired from Jackson Laboratory, matching in sex and age. Between three and five mice were housed per cage with ad libitum access to water and food. Mice were maintained in 12h:12 h light-dark cycle at constant temperature (21°C $\pm$ 2) and humidity (45% $\pm$ 5 relative humidity). All experiments were approved by the Danish Ministry of Justice and Animal Protection Committees under the permit 2017-15-0201-01241 from the Danish Animal Experiment Inspectorate.

2.2 | Treatment and tissue collection

Male and female mice from four randomized groups were studied: Placebo treated WT mice, placebo treated Tg-SwDI mice (TG), ATZ treated Tg-SwDI mice (TG+ATZ) and MTZ treated Tg-SwDI mice (TG+MTZ) (Figure 1). Treatment started at 4 months old and lasted 6 months until sacrifice. The researchers were blinded to the treatment which was performed with a special diet designed with either ATZ (Santa Cruz Biotechnology, Inc. Dallas, Texas, USA) or MTZ (Santa Cruz Biotechnology, Inc. Dallas, Texas, USA) added at a concentration of 0.01% (100 parts per million, corresponding to a 20 mg/Kg/day dose) to a standard diet (Altromin 1320; Brogaarden ApS, Lynge, DK) and produced in the same pellet form.

In line with 3R principles, tissue for the present study was collected from mice that were also part of a different study[19], see Supplementary Materials. Mice were sacrificed with an intraperitoneal overdose of pentobarbital (100 mg/kg). After harvesting the brain, the left hemisphere hippocampus and cortex were extracted, snap-frozen, and stored at a -80°C until preparation for molecular analyses.

RESEARCH IN CONTEXT

1. **Systematic review**: The authors reviewed the literature using traditional (e.g., PubMed) sources. The cited literature was focused on documenting data on the studied mouse model of dementia, and to support the biological interpretations of the experimental data.
2. **Interpretation**: Our findings led to an extensive description of the proteome changes in the brain of studied mouse model and integrated the novel data with existing literature data. Disease related pathways were chosen and drug efficacy was evaluated positive, and interpreted with respect to biological regulation of, for example, synapses.
3. **Future directions**: The manuscript documents molecular effects of a new treatment and, together with recent literature data describing the use of the same novel treatments, propose possibilities for improved pharmacological treatments of AD.

2.3 | Sample preparation

The samples from the four groups (WT, TG, TG+ATZ, and TG+MTZ) were organized in four independent proteomics studies of female hippocampus, female cortex, male hippocampus, and male cortex, with 16 samples in each (Figure 1). Protein was extracted as described preciously[19]. Briefly, frozen tissue was minced and homogenized by grinding and ultrasonication in 20 µL pr. mg tissue extraction buffer with 2% sodium dodecyl sulfate (SDS), 100 mM sodium HEPES, and protease inhibitors. Protein content of each sample was measured in triplicates with the bicinchoninic acid (BCA) assay. Within each study 40 µg protein from each sample was processed according to the TMT 16-plex manufacturer's instruction (Thermo Fisher Scientific, USA). After reduction and blocking of cysteines, and trypsin digestion, the samples were TMT labeled, pooled, fractionated by isoelectric focusing (IEF), and C18 purified as detailed in Supplementary Materials and previously described in Edhager et al.[43]

2.4 | Liquid chromatography tandem mass spectrometry analysis (LC-MS/MS)

Peptides from the ten IEF fractions of each of the four proteomics studies, were separated by nano liquid-chromatography (nLC) (Easy-nLC 1200, Thermo Scientific) coupled to a mass spectrometer (Q Exactive HF-X, Thermo Fisher Scientific, Bremen, Germany) through an EASY-Spray nano-electrospray ion source. Pre-column (Acclaim PepMap 100, 75 µm x 2 cm, Nanoviper, Thermo Scientific) and analytical column

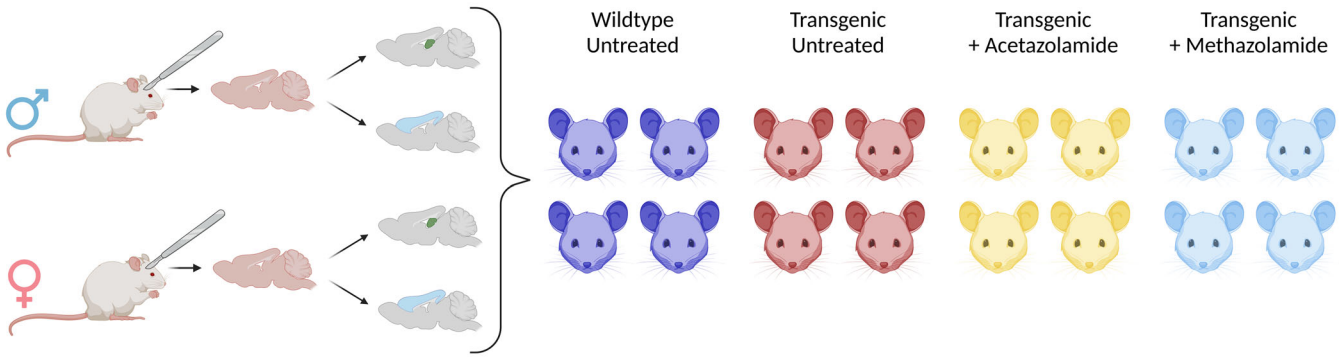

FIGURE 1 Study design. Overview of the study design. Four groups of mice were investigated: A group of WT mice receiving no treatment, and three groups of Tg-SwDI mice that were either untreated, treated with AZT, or treated with MTZ. The proteomics analyses were designed as four independent studies: Four mice of a sex were included from each group, and two tissues were analyzed from each mouse. A study as such consisted of, for example, male cortex samples from four untreated WT mice, four untreated Tg-SwDI mice, four ATZ treated Tg-SwDI mice, and four MTZ treated Tg-SwDI mice. AZT, acetazolamide; MTZ, methazolamide; WT, wild-type.

(EASY-Spray column, PepMap RSLC C18, 2 µm, 100 Å, 75 µM x 25 cm) were used to trap and separate peptides using a 170-minute gradient (5-40% acetonitrile, 0.1% formic acid). The mass spectrometer (MS) was operated in positive mode, and higher energy collisional dissociation (HCD) with collision energy (NCE) of 35 was applied for peptide fragmentation. See Supplementary Materials for further details. The mass spectrometry proteomics data have been deposited to the ProteomeXchange Consortium via the PRIDE[75] partner repository with the dataset identifier PXD055083. Table S1 contains total lists of quantitated proteins and statistical evidence.

2.5 | Bioinformatics and statistical analyses

2.5.1 | Database searches

Database searches were conducted in Proteome Discoverer 2.5 (Thermo Scientific) with Sequest algorithm on all raw files from a study merged against *Mus musculus* database from Uniprot.org containing 16,996 entries. Tryptic peptides with maximum two missed cleavages were allowed. See Supplementary Materials for further details. Subsequent bioinformatic and statistical analyses were performed in R (version 4.3.1) if not otherwise stated.

2.5.2 | Outlier removal and exclusion of keratins

Keratins were excluded from the analyses (Supplementary Materials) due to the susceptibility to contamination with these proteins during extraction and sample preparation steps.

Four samples were excluded from downstream analysis due to being outliers on the proteome level. The outliers were identified as non-grouping samples in a clustering analysis (Figure S1). In no cases did samples originate from the same mouse, suggesting a technical cause. The four excluded samples were: one from the group of TG male hippocampus, one from the TG+MTZ male hippocampus, one from the WT male cortex, and one from the TG female cortex.

2.5.3 | Clustering

Clustering was performed using the 'pheatmap' R package. The relative abundance of each protein was log2 transformed, scaled to a standard deviation of 1, and centered on 0. A complete linkage hierarchical clustering algorithm was used.

2.5.4 | DEqMS statistical analysis

Statistical analysis was performed using the 'DEqMS' R package[44] comparing either the untreated Tg-SwDI mice with the WT mice or the two treated groups of Tg-SwDI mice with the untreated Tg-SwDI mice. For each statistical comparison, a global coefficient of variance (CV) was computed by taking the average of the CV of each protein within each of the groups. We employed a fold change minimum of 2x the global CV as the biological significance criterion within a specific study and comparison to assure biologically relevant alterations. The DEqMS p-values of biologically significant proteins were corrected for multiple testing by the Benjamini–Hochberg method.

2.5.5 | Functional term analyses

The proteomap was created with the proteomap online tool[45] and layered and edited in Inkscape vector graphics software. Functional enrichment analyses of gene ontology (GO) terms were performed using the online DAVID[46] Functional Annotation Chart algorithm with default analysis settings. See Supplementary Materials for further details.

2.5.6 | General treatment effect analysis

To test for general treatment effects, proteins that were significantly dysregulated in untreated Tg-SwDI mice relative to WT mice were selected from each study and stratified by the direction of their dysregulation. Difference between the four groups in expression level of the dysregulated proteins was tested for with the Friedman Rank Sum Test, a pairwise non-parametric test able to compare more than two groups. Nemenyi's All-Pairs Comparisons Test for Unreplicated Blocked Data was used as a pairwise non-parametric post hoc analysis to identify significantly different groups and associate a significance level with the comparison between the untreated Tg-SwDI group and the two treatment groups. The *p*-values were corrected for multiple testing by the Benjamini–Hochberg method.

3 | RESULTS

The proteomes of two brain regions implicated in AD, the hippocampus and the cortex, were mapped in both females and males (Figure 1). More than 6000 unique proteins were quantified in at least one of the four studies, each composed of samples with a specific tissue and sex combination. A core of ~3600 of these were consistently quantified in all four studies (Table S1, Figure S2).

3.1 | Extensive proteome adaptations in Tg-SwDI mice

Initially, we assessed whether the presymptomatic TG tissues displayed an altered proteomics pattern compared with WT mice. Hierarchical clustering of proteins detected in all four studies almost perfectly grouped TG and WT samples (Figure 2A). This demonstrates a clear phenotype in transgenic mice at the level of the proteome, that outweighed tissue/sex similarities as well as potential analytical variance in the four independent proteomics studies.

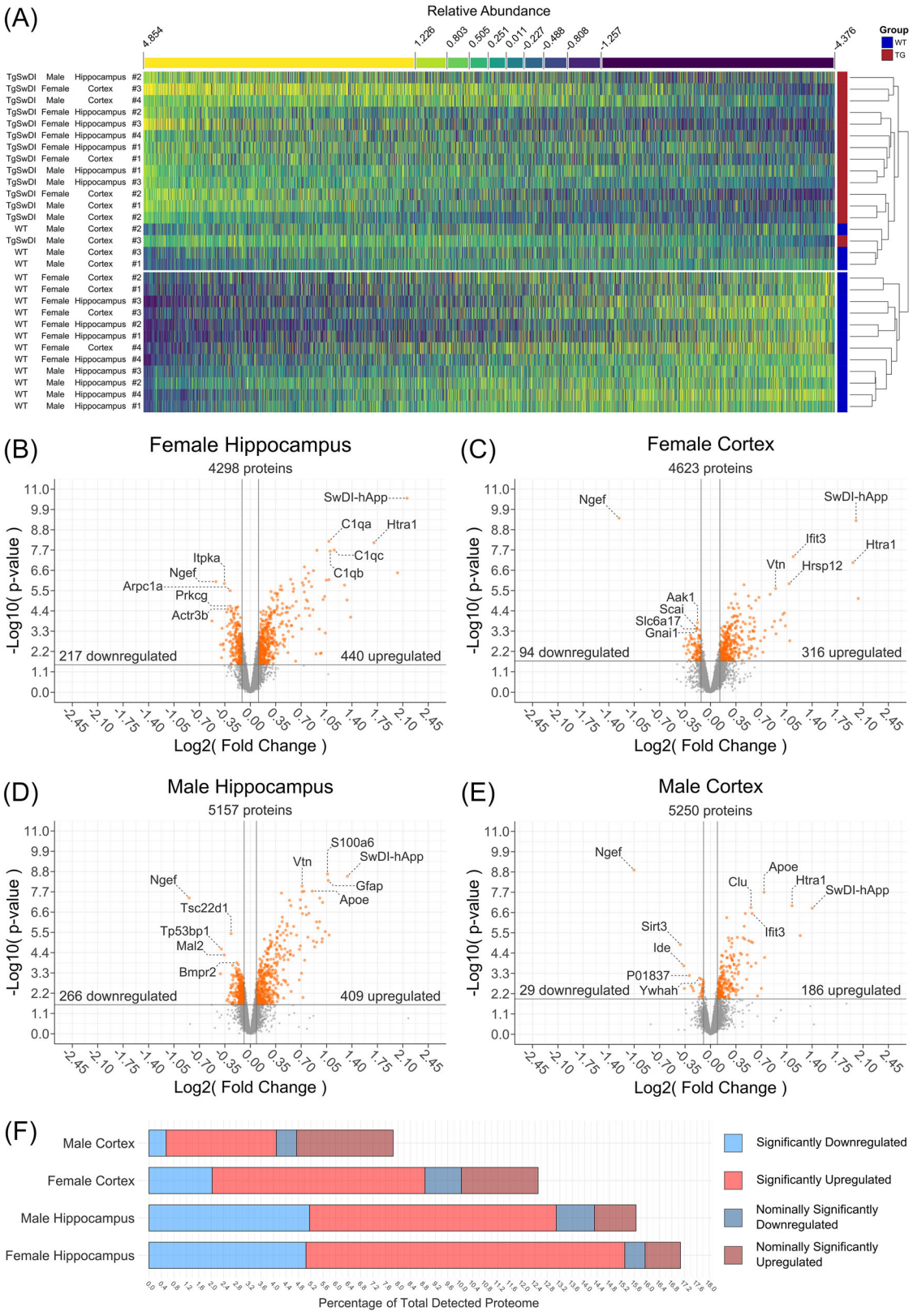

FIGURE 2 Global proteome findings of the study. (A) A complete-linkage hierarchical clustering and corresponding heatmap of the 3621 proteins quantified in all four studies. Abundances of individual proteins were log2-transformed, centered, and scaled. Color was coded according to 10% quantiles, as indicated in the heatmap legend. (B–E) Volcano plots from each individual study, with highlights of select severely dysregulated proteins. Primary axis plots log2-transformed ratio of mean abundance in the transgenic relative to the wild-type group. Secondary axis plots –log10-transformed raw p-value from the DEqMS statistical analysis. Extreme position relative to 0 on the primary and secondary axis respectively defines high level of dysregulation and high level of statistical significance. Colors indicate: gray: unregulated proteins: Not regulated

In agreement with this, statistical analyses identified hundreds of proteins in each of the individual studies displaying significant differential abundance in TG mice relative to WT mice (Figure 2B–E) referred to as dysregulated proteins.

A higher percentage of proteins were dysregulated in hippocampus tissue than in cortex, in both male and female mice, indicating a more severe affliction of the hippocampus (Figure 2F). This is consistent with findings that the hippocampus is the tissue with earliest vascular deposition of Aβ in the TG-SwDI model[14] and consistent with findings in other models describing hippocampus as an early site of functional change in AD.[47,48] We also detected sex differences with a higher percentage of dysregulated proteins in the female tissues than in their male counterparts placing hippocampus from females as the most severely affected tissue across the studies (Figure 2F). This aligns with recent reports from the Tg-SwDI model, that females are more severely affected than males both in terms of cognitive impairment and microbleeds from the cerebral vasculature and it shows that the molecular phenotype we observe aligns with clinical pathology.[17,49]

Sixty-five proteins were dysregulated in all four studies (Table 1). Among the most upregulated of these proteins were several products of AD risk genes, including Apolipoprotein E (APOE), Clusterin (CLU), murine APP (mAPP), and unsurprisingly high levels of the human transgenic APP with the SwDI mutations (SwDI-hAPP). Additionally, highly and consistently upregulated in our model was glial fibrillary acidic protein (GFAP), an astroglial marker researched as a blood biomarker for AD,[50] and Aquaporin-4 (AQP4) involved in perivascular clearance of Aβ.[51] Complement C4-B (C4B) and Complement C1Q subcomponent subunits A, B, and C (C1QA, C1QB & C1QC) were also consistently highly upregulated. Generally, more proteins were upregulated than downregulated in the studies, and just three proteins (immunoglobulin superfamily members, Ephexin-1, and Plexin-A4) were downregulated in all four studies.

Of the 65 proteins from table 1, 54 had functional annotations in the KEGG pathway database, that enabled a Proteomap[45] visualization (Figure 3). In agreement with the observations above, the term "Alzheimer's Disease" is directly identifiable. Complement takes on a prominent zone in the map, alongside several signaling pathways, not least 'Axon Guidance' signaling molecules. The map also reveals defects in several metabolic pathways including multiple enzymes involved in lipid and steroid metabolism.

3.2 | Functional enrichment of dysregulated proteins

In the core proteome of 3621 proteins quantified in all four studies, 161, 331, 476, and 563 proteins were dysregulated in male cortex, female cortex, male hippocampus, and female hippocampus, respectively. These protein lists were analyzed for enrichment of specific functional terms from the GO database. 34 GO-terms were significantly enriched in at least one study (Table S2).

To compare enriched terms across studies based not only on significance of the enrichment but also on the extent of dysregulation, we combined protein lists from all four studies from GO-terms that were enriched in any study. We then computed the MAL-FC (median of the absolute log2-transformed fold change) of the proteins in these groups as a cross-study comparative measure of term-wide level of dysregulation (Figure 4).

Female tissues, particularly the hippocampus, exhibited the highest number of enriched terms with 29 out of 34 being enriched in either of the female tissues (Figure 4). In contrast, only 10 terms out of 34 were enriched in the either of the male tissues (Figure 4). Several terms identified as enriched only in female tissues also showed elevated MAL-FC in males (Figure 4). This pattern suggests similar pathology that has not yet developed to a point of significant enrichment in male mice. Two terms, "extracellular space" and "extracellular region", were detected phenotypically enriched in all four studies, indicating that the extracellular environment is greatly influenced in both sexes and tissues (Figure 4A).

The term "glutamatergic synapse" was highly significantly enriched in female hippocampus (Figure 4A), and within this term multiple central subunits of both the α-amino-3-hydroxy-5-methyl-4-isoxazolepropionic acid (AMPA) and N-methyl-D-aspartate (NMDA) glutamatergic receptors were significantly downregulated. This included GRIA1 and GRIA2 from the AMPA receptor and GRIN1, GRIN2A, and GRIN2B from the NMDA receptor (Supplementary Table 2).

Proteins of central metabolism were also dysregulated including the above mentioned "lipid metabolic process" in both female tissues and "mitochondrion", "fatty acid metabolic process", and "oxidoreductase activity" that were dysregulated in female cortex and some alteration suggested by the MAL-FC in female hippocampus (Figure 4B). Female hippocampus on the other hand displayed more clear evidence of dysregulated calcium homeostasis with terms like "calcium ion binding", "calmodulin binding", and "sarcolemma" enriched and highly dysregulated (Figure 4A&C).

3.3 | Treatment effects

Prolonged treatment with ATZ or MTZ was recently shown to reduce AD associated pathology in the Tg-SwDI mouse model.[18,19] Thus, we wanted to substantiate the effectiveness of these drugs by (1) exploring their general effects on dysregulated proteins and (2) functionally

above the biological significance level (2x global mean of CV) and/or not significant in Benjamini–Hochberg corrected statistical test. Orange: dysregulated proteins: fold-change above biological significance level and $p > 0.05$ after Benjamini–Hochberg multiple testing correction. (F) Proportion of dysregulated proteins in each study. Nominally significant proteins (proteins that were filtered by the multiple testing correction) are shown to demonstrate that differences were not driven by differences in number of total proteins detected in the studies and in extension stringency of the multiple testing correction. CV, coefficient of variance.

TABLE 1 List of proteins significantly dysregulated in all four studies.

Accession	Gene	Description	Female hippocampus	Female cortex	Male hippocampus	Male cortex
P05067	SwDI-hApp	SwDI Human amyloid beta precursor protein	4.46	4.01	2.53	2.64
P03995	Gfap	Glial fibrillary acidic protein	4.08	4.10	2.11	2.35
Q9R118	Htra1	Serine protease HTRA1	3.25	3.90	1.83	2.18
P08226	Apoe	Apolipoprotein E	2.52	2.04	1.81	1.67
Q02105	C1qc	Complement C1q subcomponent subunit C	2.23	1.87	1.98	1.38
P20152	Vim	Vimentin	2.61	1.65	1.88	1.31
P98086	C1qa	Complement C1q subcomponent subunit A	2.12	1.68	2.05	1.37
Q64345	Ifit3	Interferon-induced protein with tetratricopeptide repeats 3	2.03	2.20	1.46	1.49
P14106	C1qb	Complement C1q subcomponent subunit B	2.14	1.81	1.56	1.39
P01029	C4b	Complement C4-B	1.74	2.13	1.65	1.25
P52760	Hrsp12	Ribonuclease UK114	2.00	2.12	1.28	1.27
P20060	Hexb	Beta-hexosaminidase subunit beta	2.07	1.61	1.67	1.23
O70370	Ctss	Cathepsin S	1.73	1.47	1.64	1.44
P29788	Vtn	Vitronectin	1.30	1.86	1.64	1.42
O08709	Prdx6	Peroxiredoxin-6	1.80	1.77	1.36	1.29
O35639	Anxa3	Annexin A3	1.74	1.45	1.61	1.25
Q06890	Clu	Clusterin	1.66	1.54	1.35	1.47
P51880	Fabp7	Fatty acid-binding protein, brain	1.54	1.51	1.60	1.35
Q61233	Lcp1	Plastin-2	1.68	1.46	1.47	1.29
P31786	Dbi	Acyl-CoA-binding protein	1.35	1.52	1.42	1.28
P05555	Itgam	Integrin alpha-M	1.47	1.40	1.46	1.22
P26041	Msn	Moesin	1.51	1.33	1.45	1.23
P55088	Aqp4	Aquaporin-4	1.46	1.38	1.43	1.25
Q9Z1Q5	Clic1	Chloride intracellular channel protein 1	1.25	1.56	1.51	1.12
Q60963	Pla2g7	Platelet-activating factor acetylhydrolase	1.27	1.59	1.20	1.20
P50114	S100b	Protein S100-B	1.33	1.46	1.21	1.21
Q3UNZ8		Quinone oxidoreductase-like protein 2	1.50	1.31	1.29	1.12
Q60766	Irgm1	Immunity-related GTPase family M protein 1	1.28	1.34	1.29	1.26
P55065	Pltp	Phospholipid transfer protein	1.69	1.21	1.10	1.16
P48036	Anxa5	Annexin A5	1.45	1.19	1.32	1.16
Q99L04	Dhrs1	Dehydrogenase/reductase SDR family member 1	1.36	1.24	1.26	1.14
O08739	Ampd3	AMP deaminase 3	1.29	1.17	1.18	1.21
Q9R062	Gyg1	Glycogenin-1	1.26	1.29	1.14	1.13
P97371	Psme1	Proteasome activator complex subunit 1	1.18	1.27	1.22	1.14
Q9Z0R9	Fads2	Fatty acid desaturase 2	1.29	1.14	1.11	1.24
Q99PL5	Rrbp1	Ribosome-binding protein 1	1.23	1.25	1.19	1.08
Q9Z275	Rlbp1	Retinaldehyde-binding protein 1	1.15	1.25	1.11	1.23
Q9Z2I8	Suclg2	Succinyl-CoA ligase [GDP-forming] subunit beta, mitochondrial	1.16	1.15	1.14	1.22
Q8K010	Oplah	5-oxoprolinase	1.21	1.16	1.10	1.16
Q07235	Serpine2	Glia-derived nexin	1.17	1.26	1.09	1.12

(Continues)

TABLE 1 (Continued)

Accession	Gene	Description	Female hippocampus	Female cortex	Male hippocampus	Male cortex
P12023	App	Amyloid beta A4 protein	1.14	1.15	1.17	1.17
Q8CI51	Pdlim5	PDZ and LIM domain protein 5	1.13	1.20	1.17	1.12
O88844	Idh1	Isocitrate dehydrogenase [NADP] cytoplasmic	1.19	1.20	1.12	1.10
P21956	Mfge8	Lactadherin	1.12	1.21	1.11	1.17
O70318	Epb41l2	Band 4.1-like protein 2	1.23	1.17	1.07	1.10
P06801	Me1	NADP-dependent malic enzyme	1.15	1.19	1.10	1.12
Q8CJH3	Plxnb1	Plexin-B1	1.16	1.22	1.07	1.10
Q61739	Itga6	Integrin alpha-6	1.14	1.14	1.17	1.10
Q00612	G6pdx	Glucose-6-phosphate 1-dehydrogenase X	1.17	1.12	1.14	1.12
Q9CQI6	Cotl1	Coactosin-like protein	1.12	1.18	1.10	1.14
Q91ZJ5	Ugp2	UTP–glucose-1-phosphate uridylyltransferase	1.13	1.15	1.14	1.11
Q91ZX7	Lrp1	Prolow-density lipoprotein receptor-related protein 1	1.10	1.18	1.08	1.17
P14231	Atp1b2	Sodium/potassium-transporting ATPase subunit beta-2	1.13	1.21	1.10	1.08
P42208	Sept2	Septin-2	1.13	1.19	1.09	1.10
P26443	Glud1	Glutamate dehydrogenase 1, mitochondrial	1.09	1.11	1.12	1.19
Q8VCW8	Acsf2	Acyl-CoA synthetase family member 2, mitochondrial	1.20	1.11	1.07	1.11
Q99JY0	Hadhb	Trifunctional enzyme subunit beta, mitochondrial	1.12	1.18	1.10	1.08
Q8BMS1	Hadha	Trifunctional enzyme subunit alpha, mitochondrial	1.14	1.16	1.10	1.07
B2RXS4	Plxnb2	Plexin-B2	1.15	1.13	1.08	1.09
O88456	Capns1	Calpain small subunit 1	1.13	1.13	1.07	1.11
P43406	Itgav	Integrin alpha-V	1.10	1.14	1.08	1.10
Q9DAK9	Phpt1	14 kDa phosphohistidine phosphatase	1.12	1.10	1.06	1.11
Q8R366	Igsf8	Immunoglobulin superfamily member 8	0.92	0.86	0.92	0.91
Q80UG2	Plxna4	Plexin-A4	0.86	0.90	0.93	0.93
Q8CHT1	Ngef	Ephexin-1	0.72	0.42	0.56	0.48

Note: List of the 65 proteins that were found to be dysregulated in all four studies independently. The table includes for each protein the Uniprot accession number, gene symbol, and description alongside the proteins' ratio of abundance in the transgenic and wild-type (WT) group. The table is ordered according to the mean of the WT ratio across the studies.

characterizing the groups of proteins these CAIs prevent dysregulation of.

3.3.1 | General proteomics effects

Within each proteomics study of a specific tissue and sex, we first investigated the general effect of the treatments on proteins that were dysregulated in the TG group compared to the WT group. These dysregulated proteins were categorized as either up- or downregulated proteins, and their relative expression levels in the TG+MTZ and TG+ATZ groups were assessed. Highly significant treatment effects were observed, and represented in all significant cases, an overall shift of expression levels of dysregulated proteins toward the expression level in WT mice, implicating that the CAI treatments impede pathological changes (Figure 5).

The most-notable effects were on downregulated proteins in hippocampus and cortex from female TG+MTZ mice (p = 2.25e-13 and p = 2.85e-13, respectively) (Figure 5A and 5B). Similar, albeit not as pronounced, effects were observed on downregulated proteins in female TG+ATZ mice (Figure 5A and 5B). We observed no significant effect on upregulated proteins in female hippocampus (Figure 5A), but in

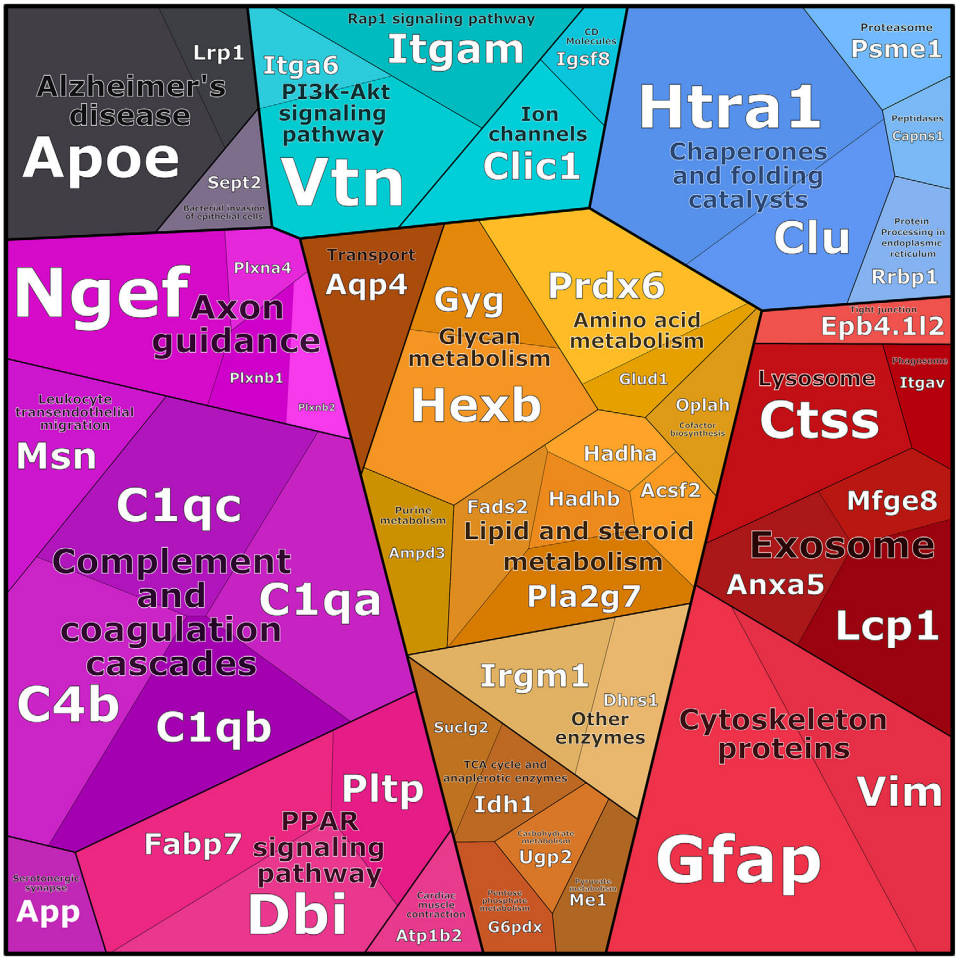

FIGURE 3 Proteomap of consistently dysregulated proteins. Proteomap of the 54 of the 65 proteins from Table 1 that had Kegg annotations enabling mapping. Areas were scaled to the mean pI-value of the four studies, that is, the product of the absolute log2 transformed fold change and the negative log10 transformed *p*-value.

female cortex, both TG+ATZ and TG+MTZ mice displayed a highly significant difference in expression level of upregulated proteins (both $p = 2.25e\text{-}13$) (Figure 5B).

In male mice, no significant effects were observed of any treatment in cortex tissue (Figure 5D). In male hippocampus, whose proteome was affected more clearly, significant positive effects in both the TG+ATZ and the TG+MTZ groups were detected on both up- ($p = 5.68e\text{-}7$ and $p = 2.21e\text{-}4$, ATZ and MTZ, respectively) and downregulated proteins ($p = 8.17e\text{-}8$ and $p = 5.41e\text{-}3$, ATZ and MTZ, respectively) (Figure 5C).

3.3.2 | Functional effects of MTZ treatment in females

Female TG mice exhibited more severe deviation from WT mice than male mice, *and* MTZ demonstrated the most substantial effects in both hippocampal and cortical tissues from females (Figure 5A&B). Given these pronounced effects, we conducted a functional enrichment analysis to explore the specific impact of MTZ treatment in the female TG mice.

To focus on normalizing effects of MTZ, only dysregulated proteins that were inversely regulated by MTZ were selected. This initial selection covered 446/657 = 68% and 364/410 = 89% of dysregulated proteins in female hippocampus and female cortex respectively. The scale of MTZ's effect on individual proteins, was assessed by the pI-value of the statistical comparison between the TG and TG+MTZ groups (pI_{MTZ}). The quartile of the selected proteins with the highest pI_{MTZ} values were investigated for functional enrichment of GO-terms.

Among the represented GO terms (Table S3) some proteins mapped to multiple terms (Figure 6A,D). Therefore, in Figure 6, we only highlight the two most significant GO-terms from female hippocampus and female cortex, respectively.

MTZ treatment first and foremost had an astounding effect on "glutamatergic synapse" proteins (Figure 6B). This term was the most significantly enriched term of any analysis of treatment effect ($p = 1.83E\text{-}06$) and notably includes subunits of both the NMDA and AMPA receptors GRIN1, GRIN2A, and GRIA1, as well as other proteins involved in glutamate and electrophysiological signaling. Additionally, a line of proteins involved in cytoskeletal dynamics in synapses are represented, HOMER3, EPHA4, and FARP1. This aligns with the second most

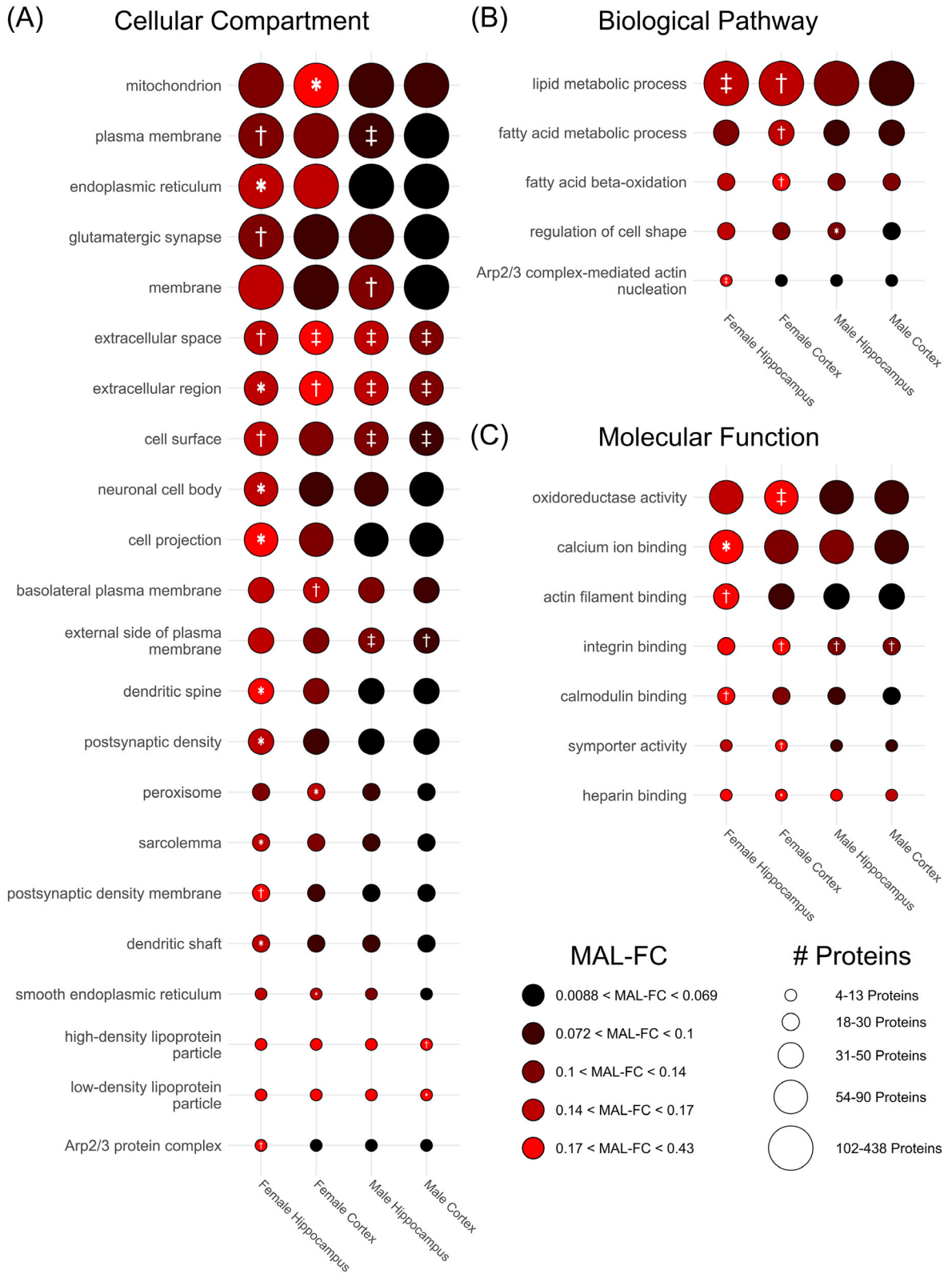

FIGURE 4 Functional enrichment analysis of dysregulated proteins. An overview of the cellular compartment (A) biological pathways (B) and molecular function (C) GO-terms that were overrepresented in the dysregulated proteins (Benjamini–Hochberg corrected p-value < 0.05) in at least one of the four studies. Circle size indicates number of proteins mapping to the term. Color scale indicates the median log2 transformed fold change of proteins in transgenic animals compared to wild type. Asterisk, dagger, and double dagger indicates p-value for overrepresentation of the term in the dysregulated proteins (* = $p < 0.05$, † = $p < 0.01$, ‡ = $p < 0.001$). Full analysis results are available in Table S2. GO, gene ontology.

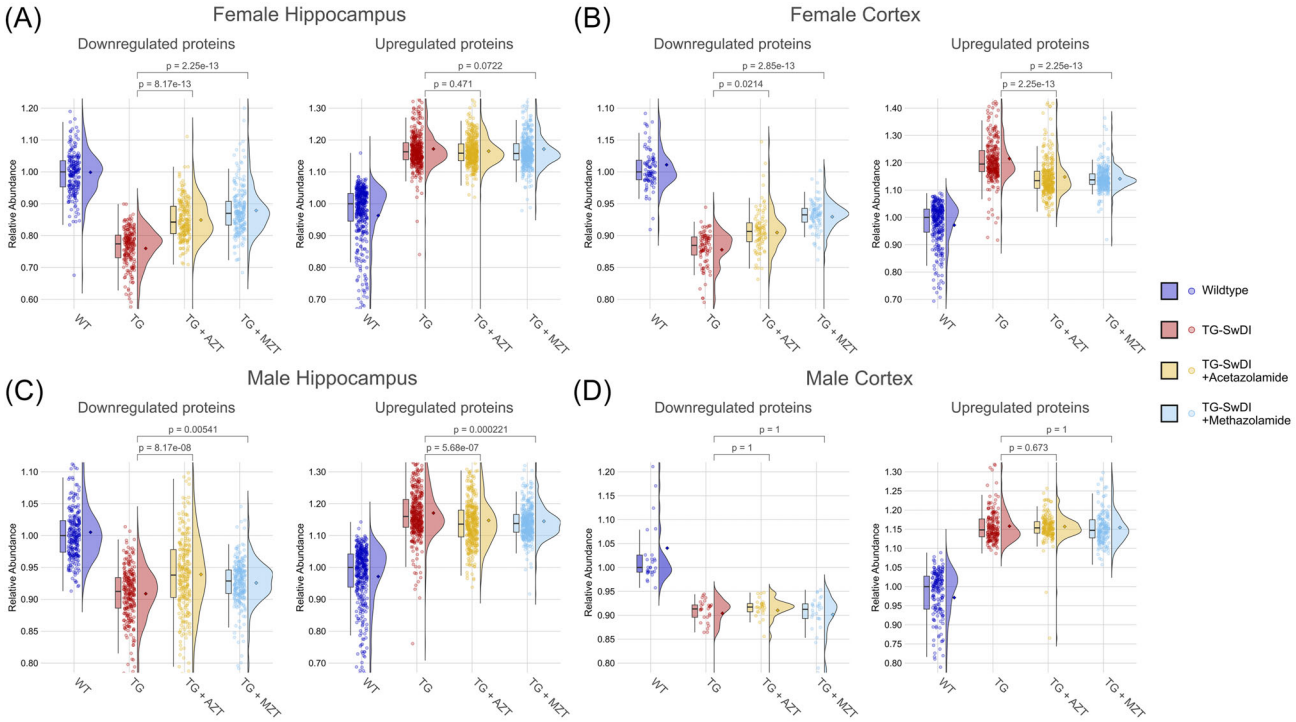

FIGURE 5 General effects of MTZ and acetazolamide treatment. In each study, (A) female hippocampus, (B) female cortex, (C) male hippocampus, and (D) male cortex, proteins that were significantly dysregulated (Untreated Tg-SwDI versus WT, multiple testing corrected $p < 0.05$) were stratified in upregulated and downregulated proteins. Differences between the untreated Tg-SwDI group versus either of two treatment groups were tested statistically by Nemenyi's all-pairs comparisons test for unreplicated blocked data – a pairwise non-parametric test. The depicted *p*-values are after correction for multiple testing by the Benjamini–Hochberg method. MTZ, methazolamide; WT, wild-type.

significant cluster being "Arp2/3 complex-mediated actin nucleation" (p = 2.64E-04) (Figure 6C).

Our further analysis into MTZ's effects revealed that it protects from the synaptic dysfunction we observe in female hippocampus. In our functional enrichment analysis of the proteins MTZ most positively affected, the top five "cellular compartment" GO-terms were "postsynaptic membrane", "synapse", "postsynapse", "dendrite", and "glutamatergic synapse". More than 80% of dysregulated "glutamatergic synapse" proteins were downregulated in the Tg-SwDI mice and a broad range of these were expressed in the MTZ treated mice at significantly more normal levels (Figure 6B).

In female cortex, we highlight the enriched terms "extracellular space" and "lysosome" (Figure 6E-F). We note that the implicated proteins were not significant individually in the analysis comparing the full proteome of MTZ treated and untreated Tg-SwDI mice. This is likely because of high variance in the untreated group in female cortex, combined with a less than complete normalizing effect of MTZ. Meanwhile, we reiterate that MTZ displayed considerable systematic reduction of dysregulation of proteins in the tissue (Figure 5B), and the terms reported here (Figure 6E&F) were significantly enriched in the quartile of dysregulated proteins where this preventive effect was most clearly demonstrated, measured on the pI_{MTZ} value.

The term "extracellular space" was most significantly enriched in female cortex (p = 1.52E-02) (Figure 6E). It includes, among others, APOE and CLU, the products of two AD risk genes, as well as complement C4B and the three complement C1Q subunits. It displayed some overlap with the 12 proteins implicated in the "lysosome" term, which encompassed the second most significant cluster in female cortex (p = 4.52E-02) (Figure 6F). The "lysosome" mapping proteins included, among others, specific degradative enzymes, cathepsin S (CTSS), cathepsin H (CTSH), and both subunits of the hexosaminidase B (HEXA and HEXB).

4 | DISCUSSION

We captured for the first time the proteomic phenotype of cortex and hippocampus tissue from the Tg-SwDI mouse model. The molecular changes were extensive in both the number of significantly altered proteins and in the degree of alterations and included known AD biomarkers. Importantly, we found that both MTZ and ATZ treatment had protective effects, maintaining more normal expression profiles of the dysregulated proteins.

4.1 | Synaptic dysfunction

In our functional enrichment analysis, GO-terms related to the function of the Arp2/3 complex, that enables the formation of branched actin filaments at the surfaces of lipid membranes, were highly

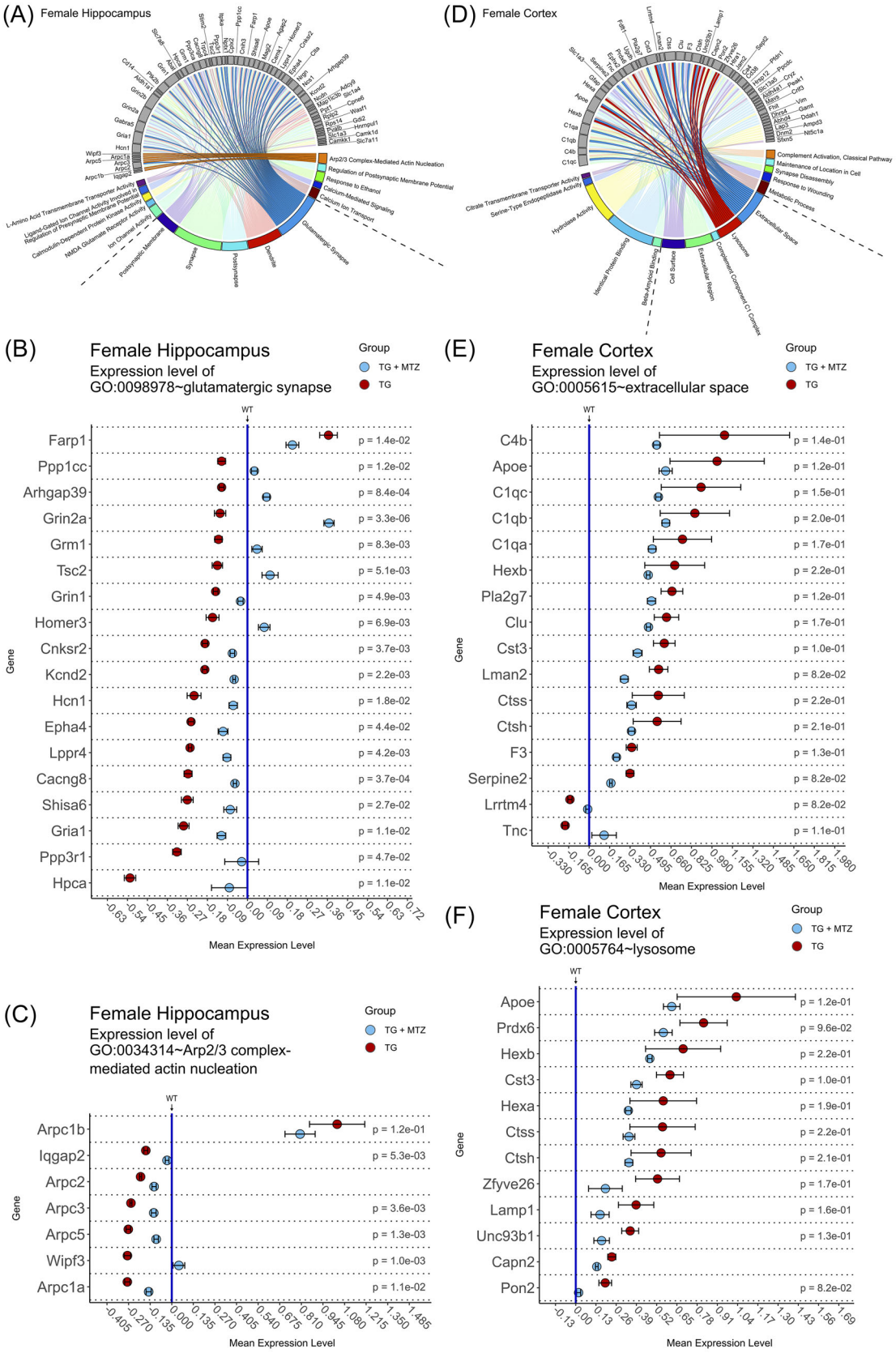

FIGURE 6 Functional enrichment analysis of MTZs protective effects in females. A detailed look at proteins and pathways that were positively affected by MTZ treatment. All proteins included in the analysis were significantly dysregulated in Tg-SwDi mice relative to WT mice. Among these dysregulated proteins the quartile with the highest pI_{MTZ} value were selected for functional enrichment analysis of GO-term in DAVID. (A,B) Chord diagrams visualizing how proteins map to different and oftentimes multiple terms. The five molecular function, five cellular compartment, and five biological pathway GO-terms with the lowest *p*-values in the functional enrichment analysis in female hippocampus (A) and female cortex (B) are plotted. Full analysis results are available in Table S3.(C–F) Expression levels of individual proteins mapped to the two most significant

significantly enriched (Figure 4A,B). The role of Arp 2/3 complex in CAA and AD has not previously been characterized but Arp3 has been described to mediate blood–brain barrier dysfunction in rats,[52] and inhibition of the Arp2/3 complex is associated with dendritic spine loss.[53] Interestingly, the GO-term "dendritic spine" was also significantly enriched and highly dysregulated in female hippocampus (Figure 4A). Memory formation and preservation is intimately connected with the formation and retraction of dendritic spines, and concomitantly deficits in a long list of activators of the Arp2/3 complex are associated with memory impairment.[54]

Interestingly, two of the three proteins downregulated in all four studies (Table 1), Plexin-A4 and Ephexin-1, are both involved in signaling pathways that activate dendritic spine retraction, and signaling through both proteins can be pathologically activated by Aβ.[55–57] Plexin-A4 is an AD risk gene product and a receptor of CLU, another well-known AD risk gene product, which we also found dysregulated (Table 1).[58] The link between AD and Ephexin-1 has been less explored but it has recently been investigated as a potential AD risk gene and associated with memory function.[59] Ephexin-1 was the most significantly and most severely downregulated protein in all four studies by far, indicating that this is an early and significant molecular adaptation. EPHA4, that initiates the signaling cascade Ephexin-1 participates in[57], was additionally downregulated in female hippocampus by almost 20% (Table S1). EPHA4 promotes spine retraction by initiating actin disassembly,[60] and in mouse models, aberrant expression of EPHA4 has been identified as a very early event in AD progression.[61]

Aberrant EPHA4/Ephexin-1 signaling could be hypothesized in the extreme to cause reduction in the overall abundance of synapse proteins and indeed in female hippocampus we observe significant enrichment of the "glutamatergic synapse" term (Figure 4A), with 82% of the dysregulated "glutamatergic synapse" proteins being downregulated. This notably includes multiple subunits of the NMDA (GRIN1, GRIN2A, and GRIN2B) and AMPA (GRIA1 and GRIA2) receptors both of which, like EPHA4, have been found to be agonistically activated by Aβ oligomers.[57]

These observations together define a profound dysfunction of glutamatergic synapses present already in the prodromal phase of development of cognitive deficits in the TgSwDI model, and potentially implicate Aβ oligomer toxicity in driving some of these pathological changes.

4.2 | Astroglia activation

Astrogliosis is a well-known hallmark of AD. In the presence of Aβ aggregates, astrocytes become reactive, pro-inflammatory, and neurotoxic.[62] Astrogliosis, is associated with increased levels of astrocyte cytoskeletal proteins such as GFAP and vimentin (VIM),[63,64] that were highly upregulated in all four studies in this model (Table 1). GFAP in particular, has recently been added as a biomarker of astrocytic activation in the criteria for diagnosis of AD.[65] Several other astroglia associated proteins were upregulated in all four studies including CLU, APOE, and the calcium-binding protein S100B (S100B), all mainly secreted from astrocytes, and AQP4 the most abundant water channel in the brain, localized at the end feet of astrocytes (Table 1).

Complement C1Q can activate astrocytes[66] and all subunits (C1QA, C1QB, and C1QC), of C1Q, as well as the complement factor C4B were highly upregulated across the four studies (Table 1). The complement system has been described to be activated in CAA[67] and C1Q specifically has been implicated in Aβ dependent microvascular damage.[68] C1Q in concert with Complement C3 is curiously also involved in early Aβ oligomer dependent synaptic pruning.[69] We note that CLU, as well as the protein Vitronectin (VTN), that are both complement inhibitors were both upregulated as well in all four studies (Table 1).[70] Together, this indicates involvement of complement dependent synaptic pruning and astrogliosis in the early pathological development in the Tg-SwDI model.

4.3 | Treatment effects

ATZ and MTZ both showed significant protective effects in male hippocampus and both female tissues (Figure 5A–C). The exemption of any treatment effect in male cortex (Figure 5D) should be viewed in the context that this tissue displayed a mild molecular phenotype and demonstrated the lowest number of significant proteins to evaluate treatment effect on. Of the two treatments MTZ was especially effective in female tissues (Figure 5A,B) while ATZ treatment was slightly more effective in male hippocampus (Figure 5C).

MTZ counteracted downregulation of proteins in the category "glutamergic synapse" (Figure 6B). This included potential drivers of the molecular pathology discussed above, notably both EPHA4 and subunits of the NMDA receptor GRIN1 and GRIN2A, but also a broad range of molecules involved in electrophysiological signaling and cytoskeletal dynamics. The effect correlated notably with a similar effect on "Arp2/3 complex-mediated actin nucleation" proteins, including five subunits of the complex itself (ARPC1A, ARPC1B, ARPC2, ARPC3, and ARPC5) and two regulatory interactors (IQGAP2 and WIPF3) (Figure 6C). Our data suggest that GRIN2A was particularly responsive to treatment with both MTZ (Figure 6B) and AZT (Table S1). In contrast, the other common glutamate binding subunit

GO-terms in female hippocampus (C,D) and female cortex (E,F). Expression levels in Tg-SwDI mice with or without MTZ treatment are shown relative to WT mice levels. Specified *p*-values indicate the level of significance of a different protein abundance in MTZ treated and untreated Tg-SwDI mice. Absent *p*-values indicate fold change below the criteria for statistical testing. Note that so many "glutamatergic synapse" proteins were in the highest pI_{MTZ} quartile that the plot of "Glutamatergic Synapse" proteins (C) was restricted, to display only the subset of mapping proteins that showed significant inverse regulation by MTZ-treatment in the proteome-wide analysis of individual proteins levels (full plot in Figure S3). GO, gene ontology; MTZ, methazolamide; WT, wild-type.

of the NMDA receptor, GRIN2B, displayed stable levels regardless of treatment (Figure S3 and Table S1). GRIN2A and GRIN2B containing receptors are reported to have different subcellular locations and opposing cellular effects, with GRIN2A being located mostly in synaptic receptors and conferring neuroprotective effects in response to excitotoxicity and Aβ-induced damage.[71,72]

In female cortex, MTZ was highly significantly effective in preventing adaptations characteristic of the TG mice (Figure 5B). Here, our functional enrichment analysis of the proteins MTZ most positively affected, identified enrichment of "extracellular space" and 'lysosome' proteins (Figure 6E,F). The "extracellular space" term included APOE, CLU and the complement factors we find dysregulated, across the four studies. In agreement with this, transcripts of many of the corrected "lysosome" proteins (Figure 6F) have been found dysregulated in reactive astrocytes from the Sod1^{G93A} mouse model of amyotrophic lateral sclerosis (ALS) by Baker et al.[73] Baker et al. also found complement proteins upregulated in the reactive astrocytes including the three C1Q subunits at both symptomatic (60 days) and late stage (90 days) disease and C4B at late stage disease.[73]

The similar profile observed in our study suggests a similar pathological state of the astroglia, and the preventive effects of MTZ treatment on the dysregulation of the implicated proteins reaffirm the preventive effects on astrogliosis, cerebrovascular, and neurovascular dysfunction that we observed in the model at the pathological and histological level[18]

5 | CONCLUSION AND PERSPECTIVES

We demonstrate in the present study the efficacy of preventive treatment with two FDA-approved CAIs, ATZ and MTZ, and thus their potential for being repurposed as AD treatments. Their benefit has recently also been demonstrated in cognitively symptomatic TgSwDI mice.[18] Treatment with these CAIs, whether for prevention or in cognitively symptomatic patients, would require prolonged use. ATZ and MTZ are generally well-tolerated in humans, but their long-term use may be associated with electrolyte imbalances (e.g., metabolic acidosis, hypokalemia) and renal effects.[74] These concerns must be considered in a risk–benefit context. Future studies may mitigate risks by identifying patient populations most likely to benefit from CAI treatment, and optimizing dosing strategies, such as intermittent administration, may help reduce adverse effects while preserving neuroprotective benefits. In the present study, MTZ notably had profound effects on glutamatergic synapse proteins, that we observed in the hippocampus of female Tg-SwDI mice. A currently employed symptomatic AD treatment, Memantine, antagonizes overstimulation of the glutamatergic NMDA receptor and interestingly, the preventive effects of MTZ treatment included maintenance of more normal levels of NMDA receptor subunits. Memantine's mode of action and effect in humans considered, our data suggest that CAI treatment effects identified here would translate in a meaningful way to combat human disease development. The effects of MTZ and ATZ are notably demonstrated in this model with severe CAA pathology and has been shown to directly ameliorate vascular pathology[18,19], suggesting CAIs' potential also as a complementary treatment to immunotherapies, possibly able to reduce antibody-induced adverse events involving vascular pathology. Our results most significantly support direct preventive effects of CAIs, on early molecular pathology associated with AD, and as both MTZ and ATZ are FDA approved for several diagnoses and safe for extended use in humans, trialing these drugs in human AD is now of high interest.

6 | LIMITATIONS

The study investigates molecular phenotypic changes and treatment responses by bulk proteomics analysis. With this approach, some protein alterations in specific anatomical structures might be missed. Moreover, the number of replicates possible to include in each proteomics study (tissue-sex-combination) limits the statistical power in the study and might lead to false negatives. Despite these limitations, a multitude of statistically significant protein and pathway alterations were identified. The significant alterations were furthermore strengthened by coherence with literature yielding high confidence in the central conclusions. The employed TMT-labeling did not allow direct, statistical, comparison of protein levels between studies, that is, between sexes or tissue types. As the results subsequently indicated the relevance of this comparison, this limitation was partly handled by normalization to WT and by comparing significant pathway alterations between the studies. Finally, the studies were performed in mice with early-stage disease and relatively limited phenotypical symptoms, and care should be taken to transfer the conclusions to late-stage disease. Group-wise differences in age were noted but deemed not to confound conclusions as assessed in Figure S4.

AUTHOR CONTRIBUTIONS

Johan Palmfeldt and Jasper Carlsen established the proteomics study objectives, designed and performed the proteomics experiments, bioinformatical analyses and data interpretations. Jasper Carlsen performed statistical analyses and wrote the first draft of the manuscript with supervision from Johan Palmfeldt. Eugenio Gutiérrez-Jiménez, Silvia Fossati and Leif Østergaard contributed to design and objectives of the animal studies and critically evaluated the manuscript. Eugenio Gutiérrez-Jiménez planned and performed animal studies and contributed to data interpretations.

ACKNOWLEDGMENTS

We thank Anna Bay and Susanne Smith Christensen for their valuable support with the sample collection. We thank John and Birthe Meyer foundation (J.P.) for financing the mass spectrometry equipment, and the following for financial support of the studies; Alzheimer's Association, (AARF-18-564411 to E.G.J.), VELUX Foundation (ARCADIA II Grant 0026167 to E.G.J., L.Ø.), NIH R01NS104127 (S.F.), R01AG062572 (S.F.), and Lundbeck Foundation (BRAIN COMET, R310-2018-3455, E.G.J., L.Ø.).

CONFLICT OF INTEREST STATEMENT

The authors declare no conflict of interest. Silvia Fossati is an inventor on US Patent 10780094 for the use of CAIs in Alzheimer's disease and CAA. All other authors have nothing to disclose in relation to this study.

DATA AVAILABILITY STATEMENT

The mass spectrometry proteomics data have been deposited to the ProteomeXchange Consortium via the PRIDE[75] partner repository with the dataset identifier PXD055083. Supplementary table 1 contains total lists of quantitated proteins and statistical evidence.

CONSENT STATEMENT

No human subjects were included in the studies so consent statements were not required.

ORCID

Jasper Carlsen https://orcid.org/0000-0001-6175-0110
Silvia Fossati https://orcid.org/0000-0002-2047-222X
Leif Østergaard https://orcid.org/0000-0003-2930-6997
Eugenio Gutiérrez-Jiménez https://orcid.org/0000-0002-7509-0720

REFERENCES

1. Collaborators GBDDF. Estimation of the global prevalence of dementia in 2019 and forecasted prevalence in 2050: an analysis for the global burden of disease study 2019. *Lancet Public Health*. 2022;7(2):e105-e125. doi:10.1016/S2468-2667(21)00249-8
2. 2020 Alzheimer's disease facts and figures. *Alzheimers Dement*. 2020;16(3):391-460. doi:10.1002/alz.12068
3. Guo T, Zhang D, Zeng Y, Huang TY, Xu H, Zhao Y. Molecular and cellular mechanisms underlying the pathogenesis of Alzheimer's disease. *Mol Neurodegener*. 2020;15(1):40. doi:10.1186/s13024-020-00391-7
4. Masters CL, Simms G, Weinman NA, Multhaup G, McDonald BL, Beyreuther K. Amyloid plaque core protein in Alzheimer disease and Down syndrome. *Proc Natl Acad Sci U S A*. 1985;82(12):4245-4249. doi:10.1073/pnas.82.12.4245
5. Glenner GG, Wong CW. Alzheimer's disease: initial report of the purification and characterization of a novel cerebrovascular amyloid protein. *Biochem Biophys Res Commun*. 1984;120(3):885-890. doi:10.1016/s0006-291x(84)80190-4
6. Brain J, Greene L, Tang EYH, et al. Cardiovascular disease, associated risk factors, and risk of dementia: an umbrella review of meta-analyses. *FrontEpidemiol*. 2023;3:1095236. doi:10.3389/fepid.2023.1095236. Review.
7. Carey A, Fossati S. Hypertension and hyperhomocysteinemia as modifiable risk factors for Alzheimer's disease and dementia: new evidence, potential therapeutic strategies, and biomarkers. *Alzheimers Dement*. 2023;19(2):671-695. doi:10.1002/alz.12871
8. Jakel L, De Kort AM, Klijn CJM, Schreuder F, Verbeek MM. Prevalence of cerebral amyloid angiopathy: a systematic review and meta-analysis. *Alzheimers Dement*. 2022;18(1):10-28. doi:10.1002/alz.12366
9. Cordonnier C, van der Flier WM. Brain microbleeds and Alzheimer's disease: innocent observation or key player?. *Brain*. 2011;134(Pt 2):335-344. doi:10.1093/brain/awq321
10. Kim SH, Ahn JH, Yang H, Lee P, Koh GY, Jeong Y. Cerebral amyloid angiopathy aggravates perivascular clearance impairment in an Alzheimer's disease mouse model. *Acta Neuropathol Commun*. 2020;8(1):181. doi:10.1186/s40478-020-01042-0
11. Greenberg SM, Bacskai BJ, Hernandez-Guillamon M, Pruzin J, Sperling R, van Veluw SJ. Cerebral amyloid angiopathy and Alzheimer disease—one peptide, two pathways. *Nat Rev Neurol*. 2020;16(1):30-42. doi:10.1038/s41582-019-0281-2
12. Gatti L, Tinelli F, Scelzo E, et al. Understanding the pathophysiology of cerebral amyloid angiopathy. *Int J Mol Sci*. 2020;21(10). doi:10.3390/ijms21103435
13. Malek-Ahmadi M, Chen K, Perez SE, Mufson EJ. Cerebral amyloid angiopathy and neuritic plaque pathology correlate with cognitive decline in elderly non-demented individuals. *J Alzheimers Dis*. 2019;67(1):411-422. doi:10.3233/JAD-180765
14. Davis J, Xu F, Deane R, et al. Early-onset and robust cerebral microvascular accumulation of amyloid beta-protein in transgenic mice expressing low levels of a vasculotropic Dutch/Iowa mutant form of amyloid beta-protein precursor. *J Biol Chem*. 2004;279(19):20296-20306. doi:10.1074/jbc.M312946200
15. Miao J, Xu F, Davis J, Otte-Holler I, Verbeek MM, Van Nostrand WE. Cerebral microvascular amyloid beta protein deposition induces vascular degeneration and neuroinflammation in transgenic mice expressing human vasculotropic mutant amyloid beta precursor protein. *Am J Pathol*. 2005;167(2):505-515. doi:10.1016/s0002-9440(10)62993-8
16. Tan NA, Carpio AMA, Heller HC, Pittaras EC. Behavioral and neuronal characterizations, across ages, of the TgSwDI mouse model of Alzheimer's Disease. *Genes-Basel*. 2024;15(1):47. doi:10.3390/genes15010047
17. Setti SE, Flanigan T, Hanig J, Sarkar S. Assessment of sex-related neuropathology and cognitive deficits in the Tg-SwDI mouse model of Alzheimer's disease. *Behav Brain Res*. 2022;428:113882. doi:10.1016/j.bbr.2022.113882
18. Canepa E, Parodi-Rullan R, Vazquez-Torres R, et al. FDA-approved carbonic anhydrase inhibitors reduce amyloid beta pathology and improve cognition, by ameliorating cerebrovascular health and glial fitness. *Alzheimers Dement*. 2023;19(11):5048-5073. doi:10.1002/alz.13063
19. Gutierrez-Jimenez E, Rasmussen PM, Mikkelsen IK, et al>. Carbonic anhydrase inhibitors prevent presymptomatic capillary flow disturbances in a model of cerebral amyloidosis. *bioRxiv*. 2024. doi:10.1101/2024.08.22.609091
20. Searcy JL, Le Bihan T, Salvadores N, McCulloch J, Horsburgh K. Impact of age on the cerebrovascular proteomes of wild-type and Tg-SwDI mice. *PLoS One*. 2014;9(2):e89970. doi:10.1371/journal.pone.0089970
21. Situ M, Citalan-Madrid AF, Stamatovic SM, Keep RF, Andjelkovic AV. Transcriptomic profile of blood-brain barrier remodeling in cerebral amyloid angiopathy. *Front Cell Neurosci*. 2022;16:931247. doi:10.3389/fncel.2022.931247
22. Zhou G, Xiang T, Xu Y, et al. Fruquintinib/HMPL-013 ameliorates cognitive impairments and pathology in a mouse model of cerebral amyloid angiopathy (CAA). *Eur J Pharmacol*. 2023;939:175446. doi:10.1016/j.ejphar.2022.175446
23. Schemmert S, Camargo LC, Honold D, et al. In vitro and in vivo efficacies of the linear and the cyclic version of an all-d-enantiomeric peptide developed for the treatment of Alzheimer's Disease. *Int J Mol Sci*. 2021;22(12):6553. doi:10.3390/ijms22126553
24. Petrushina I, Hovakimyan A, Harahap-Carrillo IS, et al. Characterization and preclinical evaluation of the cGMP grade DNA based vaccine, AV-1959D to enter the first-in-human clinical trials. *Neurobiol Dis*. 2020;139:104823. doi:10.1016/j.nbd.2020.104823
25. Scholtzova H, Do E, Dhakal S, et al. Innate immunity stimulation via toll-like receptor 9 ameliorates vascular amyloid pathology in Tg-SwDI mice with associated cognitive benefits. *J Neurosci*. 2017;37(4):936-959. doi:10.1523/JNEUROSCI.1967-16.2016
26. Saito S, Yamamoto Y, Maki T, et al. Taxifolin inhibits amyloid-beta oligomer formation and fully restores vascular integrity and memory in cerebral amyloid angiopathy. *Acta Neuropathol Commun*. 2017;5(1):26. doi:10.1186/s40478-017-0429-5

27. Ziehm T, Brener O, van Groen T, et al. Increase of positive net charge and conformational rigidity enhances the efficacy of d-Enantiomeric peptides designed to eliminate cytotoxic abeta species. *ACS Chem Neurosci*. 2016;7(8):1088-1096. doi:10.1021/acschemneuro.6b00047
28. Hattori Y, Maki T, Saito S, Yamamoto Y, Nagatsuka K, Ihara M. Influence of low-dose aspirin on cerebral amyloid angiopathy in mice. *J Alzheimers Dis*. 2016;52(3):1037-1045. doi:10.3233/JAD-160013
29. Maki T, Okamoto Y, Carare RO, et al. Phosphodiesterase III inhibitor promotes drainage of cerebrovascular beta-amyloid. *Ann Clin Transl Neurol*. 2014;1(8):519-533. doi:10.1002/acn3.79
30. Liang J, Lopez-Valdes HE, Martinez-Coria H, et al. Dihydromyricetin ameliorates behavioral deficits and reverses neuropathology of transgenic mouse models of Alzheimer's disease. *Neurochem Res*. 2014;39(6):1171-1181. doi:10.1007/s11064-014-1304-4
31. Fan R, Xu F, Previti ML, et al. Minocycline reduces microglial activation and improves behavioral deficits in a transgenic model of cerebral microvascular amyloid. *J Neurosci*. 2007;27(12):3057-3063. doi:10.1523/JNEUROSCI.4371-06.2007
32. Filippi M, Cecchetti G, Spinelli EG, Vezzulli P, Falini A, Agosta F. Amyloid-related imaging abnormalities and beta-amyloid-targeting antibodies: a systematic review. *JAMA Neurol*. 2022;79(3):291-304. doi:10.1001/jamaneurol.2021.5205
33. Perosa V, Oltmer J, Munting LP, et al. Perivascular space dilation is associated with vascular amyloid-beta accumulation in the overlying cortex. *Acta Neuropathol*. 2022;143(3):331-348. doi:10.1007/s00401-021-02393-1
34. Greenberg SM, Cordonnier C, Schneider JA, et al. Off-label use of aducanumab for cerebral amyloid angiopathy. *Lancet Neurol*. 2021;20(8):596-597. doi:10.1016/S1474-4422(21)00213-1
35. Cummings J, Aisen P, Apostolova LG, Atri A, Salloway S, Weiner M. Aducanumab: appropriate use recommendations. *J Prev Alzheimers Dis*. 2021;8(4):398-410. doi:10.14283/jpad.2021.41
36. Mishra CB, Tiwari M, Supuran CT. Progress in the development of human carbonic anhydrase inhibitors and their pharmacological applications: where are we today?. *Med Res Rev*. 2020;40(6):2485-2565. doi:10.1002/med.21713
37. Huang L, Yang Q, Zhang L, Chen X, Huang Q, Wang H. Acetazolamide improves cerebral hemodynamics in CADASIL. *J Neurol Sci*. 2010;292(1-2):77-80. doi:10.1016/j.jns.2010.01.023
38. Fossati S, Giannoni P, Solesio ME, et al. The carbonic anhydrase inhibitor methazolamide prevents amyloid beta-induced mitochondrial dysfunction and caspase activation protecting neuronal and glial cells in vitro and in the mouse brain. *Neurobiol Dis*. 2016;86:29-40. doi:10.1016/j.nbd.2015.11.006
39. Anzovino A, Canepa E, Alves M, Lemon NL, Carare RO, Fossati S. Amyloid beta oligomers activate death receptors and mitochondria-mediated apoptotic pathways in cerebral vascular smooth muscle cells; protective effects of carbonic anhydrase inhibitors. *Cells-Basel*. 2023;12(24):2840. doi:10.3390/cells12242840
40. Lemon N, Canepa E, Ilies MA, Fossati S. Carbonic anhydrases as potential targets against neurovascular unit dysfunction in Alzheimer's Disease and stroke. *Front Aging Neurosci*. 2021;13:772278. doi:10.3389/fnagi.2021.772278
41. Solesio ME, Peixoto PM, Debure L, et al. Carbonic anhydrase inhibition selectively prevents amyloid beta neurovascular mitochondrial toxicity. *Aging Cell*. 2018;17(4):e12787. doi:10.1111/acel.12787
42. Thiry A, Dogné J, Supuran CT, Masereel B. Carbonic anhydrase inhibitors as anticonvulsant agents. *Curr Top Med Chem*. 2007;7(9):855-864. doi:10.2174/156802607780636726
43. Edhager AV, Povlsen JA, Lofgren B, Botker HE, Palmfeldt J. Proteomics of the rat myocardium during development of type 2 diabetes mellitus reveals progressive alterations in major metabolic pathways. *J Proteome Res*. 2018;17(7):2521-2532. doi:10.1021/acs.jproteome.8b00276
44. Zhu Y, Orre LM, Zhou Tran Y, et al. DEqMS: a Method for accurate variance estimation in differential protein expression analysis. *Mol Cell Proteomics*. 2020;19(6):1047-1057. doi:10.1074/mcp.TIR119.001646
45. Liebermeister W, Noor E, Flamholz A, Davidi D, Bernhardt J, Milo R. Visual account of protein investment in cellular functions. *P Natl Acad Sci USA*. 2014;111(23):8488-8493. doi:10.1073/pnas.1314810111
46. Huang da W, Sherman BT, Lempicki RA. Systematic and integrative analysis of large gene lists using DAVID bioinformatics resources. *Nat Protoc*. 2009;4(1):44-57. doi:10.1038/nprot.2008.211
47. Busche MA, Chen X, Henning HA, et al. Critical role of soluble amyloid-beta for early hippocampal hyperactivity in a mouse model of Alzheimer's disease. *Proc Natl Acad Sci U S A*. 2012;109(22):8740-8745. doi:10.1073/pnas.1206171109
48. Anastacio HTD, Matosin N, Ooi L. Neuronal hyperexcitability in Alzheimer's disease: what are the drivers behind this aberrant phenotype?. *Transl Psychiat*. 2022;12(1):257. doi:10.1038/s41398-022-02024-7
49. Maniskas ME, Mack AF, Morales-Scheihing D, et al. Sex differences in a murine model of cerebral amyloid angiopathy. *Brain Behav Immun-Hl*. 2021;14:100260. doi:10.1016/j.bbih.2021.100260
50. Kim KY, Shin KY, Chang KA. GFAP as a potential biomarker for Alzheimer's Disease: a systematic review and meta-analysis. *Cells-Basel*. 2023;12(9):1309. doi:10.3390/cells12091309
51. Simon M, Wang MX, Ismail O, et al. Loss of perivascular aquaporin-4 localization impairs glymphatic exchange and promotes amyloid β plaque formation in mice. *Alzheimers Res Ther*. 2022;14(1):59. doi:10.1186/s13195-022-00999-5
52. Yan R, Liu H, Lv F, Deng Y, Li Y. Rac1/Wave2/Arp3 pathway mediates rat blood-brain barrier dysfunction under simulated microgravity based on proteomics strategy. *Int J Mol Sci*. 2021;22(10):5165. doi:10.3390/ijms22105165
53. Hotulainen P, Llano O, Smirnov S, et al. Defining mechanisms of actin polymerization and depolymerization during dendritic spine morphogenesis. *J Cell Biol*. 2009;185(2):323-339. doi:10.1083/jcb.200809046
54. Pelucchi S, Stringhi R, Marcello E. Dendritic Spines in Alzheimer's Disease: how the actin cytoskeleton contributes to synaptic failure. *Int J Mol Sci*. 2020;21(3):908. doi:10.3390/ijms21030908
55. Fu WY, Chen Y, Sahin M, et al. Cdk5 regulates EphA4-mediated dendritic spine retraction through an ephexin1-dependent mechanism. *Nat Neurosci*. 2007;10(1):67-76. doi:10.1038/nn1811
56. Chung S, Yang J, Kim HJ, et al. Plexin-A4 mediates amyloid-β-induced tau pathology in Alzheimer's disease animal model. *Prog Neurobiol*. 2021;203:102075. doi:10.1016/j.pneurobio.2021.102075
57. Vargas LM, Cerpa W, Muñoz FJ, Zanlungo S, Alvarez AR. Amyloid-β oligomers synaptotoxicity: the emerging role of EphA4/c-Abl signaling in Alzheimer's disease. *Bba-Mol Basis Dis*. 2018;1864(4):1148-1159. doi:10.1016/j.bbadis.2018.01.023
58. Kang SS, Kurti A, Wojtas A, et al. Identification of plexin A4 as a novel clusterin receptor links two Alzheimer's disease risk genes. *Hum Mol Genet*. 2016;25(16):3467-3475. doi:10.1093/hmg/ddw188
59. Hudgins AD, Zhou S, Arey RN, Rosenfeld MG, Murphy CT, Suh Y. A systems biology-based identification and in vivo functional screening of Alzheimer's disease risk genes reveal modulators of memory function. *Neuron*. 2024;112(13):2112-2129.e4. doi:10.1016/j.neuron.2024.04.009
60. Zhou L, Jones EV, Murai KK. EphA signaling promotes actin-based dendritic spine remodeling through slingshot phosphatase. *J Biol Chem*. 2012;287(12):9346-9359. doi:10.1074/jbc.M111.302802
61. Simón AM, de Maturana RL, Ricobaraza A, et al. Early changes in hippocampal eph receptors precede the onset of memory decline in mouse models of Alzheimer's Disease. *J Alzheimers Dis*. 2009;17(4):773-786. doi:10.3233/Jad-2009-1096
62. Kang WF, Balordi F, Su N, Chen L, Fishell G, Hébert JM. Astrocyte activation is suppressed in both normal and injured brain by FGF signaling.

P Natl Acad Sci USA. 2014;111(29):E2987-E2995. doi:10.1073/pnas.1320401111
63. Kim J, Yoo ID, Lim J, Moon JS. Pathological phenotypes of astrocytes in Alzheimer's disease. *Exp Mol Med*. 2024;56(1):95-99. doi:10.1038/s12276-023-01148-0
64. Dai DL, Li MY, Lee EB. Human Alzheimer's disease reactive astrocytes exhibit a loss of homeostastic gene expression. *Acta Neuropathol Com*. 2023;11(1):127. doi:10.1186/s40478-023-01624-8
65. Jack CR Jr, Andrews JS, Beach TG, et al. Revised criteria for diagnosis and staging of Alzheimer's disease: alzheimer's association workgroup. *Alzheimers Dement*. 2024;20(8):5143-5169. doi:10.1002/alz.13859
66. Dejanovic B, Wu T, Tsai MC, et al. Complement C1q-dependent excitatory and inhibitory synapse elimination by astrocytes and microglia in Alzheimer's disease mouse models. *Nature Aging*. 2022;2(9):837-850. doi:10.1038/s43587-022-00281-1
67. Matsuo K, Shindo A, Niwa A, et al. Complement activation in capillary cerebral amyloid angiopathy. *Dement Geriatr Cogn Disord*. 2017;44(5-6):343-353. doi:10.1159/000486091
68. Hu MY, Li TM, Ma XM, et al. Macrophage lineage cells-derived migrasomes activate complement-dependent blood-brain barrier damage in cerebral amyloid angiopathy mouse model. *Nat Commun*. 2023;14(1):3945. doi:10.1038/s41467-023-39693-x
69. Hong S, Beja-Glasser VF, Nfonoyim BM, et al. Complement and microglia mediate early synapse loss in Alzheimer mouse models. *Science*. 2016;352(6286):712-716. doi:10.1126/science.aad8373
70. Menny A, Lukassen MV, Couves EC, Franc V, Heck AJR, Bubeck D. Structural basis of soluble membrane attack complex packaging for clearance. *Nat Commun*. 2021;12(1):6086. doi:10.1038/s41467-021-26366-w
71. Liu YT, Wong TP, Aarts M, et al. NMDA receptor subunits have differential roles in mediating excitotoxic neuronal death both and. *J Neurosci*. 2007;27(11):2846-2857. doi:10.1523/Jneurosci.0116-07.2007
72. Raïch I, Lillo J, Rebassa JB, et al. Dual role of NMDAR containing NR2A and NR2B subunits in Alzheimer's Disease. *Int. J Mol Sci*. 2024;25(9):4757. doi:10.3390/ijms25094757
73. Baker DJ, Blackburn DJ, Keatinge M, et al. Lysosomal and phagocytic activity is increased in astrocytes during disease progression in the SOD1 G93A mouse model of amyotrophic lateral sclerosis. *Front cell neurosci*. 2015;9:410. doi:10.3389/fncel.2015.00410
74. Swenson ER. Safety of carbonic anhydrase inhibitors. *Expert Opin Drug Saf*. 2014;13(4):459-472. doi:10.1517/14740338.2014.897328
75. Perez-Riverol Y, Bai J, Bandla C, et al. The PRIDE database resources in 2022: a hub for mass spectrometry-based proteomics evidences. *Nucleic Acids Res*. 2022;50(D1):D543-D552. doi:10.1093/nar/gkab1038

SUPPORTING INFORMATION

Additional supporting information can be found online in the Supporting Information section at the end of this article.

How to cite this article: Carlsen J, Fossati S, Østergaard L, Gutiérrez-Jiménez E, Palmfeldt J. Cerebral proteome adaptations to amyloid angiopathy are prevented by carbonic anhydrase inhibitors. *Alzheimer's Dement*. 2025;21:e70122. https://doi.org/10.1002/alz.70122